coatings

MDPI

Article

Effect of Aging Time on Microstructure and Properties of Cold-Rolled Ni-W-Co-Ta Medium–Heavy Alloy

Yong Li [1], Yi Xiong [2,3,*], Hua-fei Li [2], Shun Han [1], Feng-zhang Ren [2,3] and Chun-xu Wang [1]

[1] Central Iron and Steel Research Institute, Beijing 100081, China; liysea@163.com (Y.L.); hanshun@nercast.com (S.H.); wcxu1@163.com (C.-x.W.)
[2] School of Materials Science and Engineering, Henan University of Science and Technology, Luoyang 471023, China; 15070925180@163.com (H.-f.L.); lyrenfz@163.com (F.-z.R.)
[3] Collaborative Innovation Center of New Nonferrous Metal Materials and Advanced Processing Technology Jointly Established by the Ministry of Science and Technology, Luoyang 471023, China
* Correspondence: xy_hbdy@163.com

Abstract: A systematical exploration of the effect of aging time on the microstructure and mechanical properties of cold-rolled Ni-W-Co-Ta medium–heavy alloy with 90% thickness reduction at the aging temperature of 700 °C was performed. The results demonstrate that the volume fraction of the precipitation (Ni_4W), which persists under various aging times, increases from 13.7% (2 h) to 28.7% (32 h) with the extension of aging time. Meanwhile, the microstructure after aging treatment is still dominated by dislocation entanglement and dislocation walls, although the degree of lattice distortion and dislocation density attributed to heavy deformation decreases. The maximum tensile strength, yield strength, and microhardness (2286 MPa, 1989 MPa, 766 HV) of the cold-rolled Ni-W-Co-Ta medium–heavy alloy under the 16 h aging treatment at 700 °C are reached, respectively. The ductile–brittle mixed fracture morphology is maintained in the fracture morphology of the medium–heavy alloy before and after aging treatment.

Keywords: cold-rolled Ni-W-Co-Ta medium–heavy alloy; aging time; microstructure; mechanical properties

Citation: Li, Y.; Xiong, Y.; Li, H.-f.; Han, S.; Ren, F.-z.; Wang, C.-x. Effect of Aging Time on Microstructure and Properties of Cold-Rolled Ni-W-Co-Ta Medium–Heavy Alloy. *Coatings* **2024**, *14*, 230. https://doi.org/10.3390/coatings14020230

Academic Editors: Nigel Jennett, Mingwen Bai and Elena Villa

Received: 17 January 2024
Revised: 7 February 2024
Accepted: 14 February 2024
Published: 16 February 2024

1. Introduction

The demand for medium–heavy alloys with high penetration capability, moderate strength, toughness, and critical shear strain rate, particularly in the context of warhead materials, is well established [1–3]. However, the high porosity and weak two-phase bonding of traditional medium–heavy alloys, generated by powder metallurgy methods [3–5], lead to poor comprehensive mechanical properties hardly applying to harsh service environments. In addition, the comprehensive mechanical properties cannot yet fully meet the increasingly demanding service environment, although hot rolling [6], thermostatic extrusion and the thermal torsion process [7], hot extrusion [8], and other hot deformation methods effectively mitigate the shortcomings of high porosity and weak two-phase bonding of medium–heavy alloy [9]. Therefore, Ni-W-Co-Ta medium–heavy alloys with excellent comprehensive mechanical properties, abandoning the traditional powder metallurgy method, are prepared with the approach of smelting, casting and forging for the first time in our team. However, enhanced strength by cold rolling was realized on the deterioration of the ductility, posing challenges for practical engineering applications [10]. As a result, the focus of research shifted towards developing methods to improve the comprehensive mechanical properties of the cold-rolled Ni-W-Co-Ta medium–heavy alloy.

It is widely recognized that metal materials undergo substantial dislocation formation following cold rolling. The strength of metal materials could be enhanced considerably under the effect of rapid precipitation of the second phase because of a large number of nucleation sites arising from the substructural defects after cold rolling. Therefore,

the appropriate aging treatment of cold-deformed samples can not only diminish the deformation energy storage of deformed samples but also foster the precipitation of the strengthening phase to achieve a favorable synergy between mechanical properties and ductility. For example, Zhang et al. [11] examined the effect of cold-rolling deformation and aging treatment on the mechanical properties of Cu-0.45Cr-0.14Ti (wt%) alloys and concluded that the time required for the alloys to reach maximum strength is shorter as the degree of deformation increases. A similar conclusion, that higher strength and a shorter time to reach maximum strength was obtained with the greater deformation after aging treatment on Ti-Nb-Zr alloy, was drawn by He et al. [12]. Sadeghi-Nezhad et al. [13] conducted a study on AA2024 alloy, whereby they reached the conclusion that the rolling and aging treatment possessed the capability to augment the mechanical properties of the alloy. Additionally, their findings posited that heightened deformation yielded more pronounced enhancements in the alloy's mechanical characteristics. Research findings of Xia et al. [14] further substantiated that the ultimate tensile strength of the Fe-Si-Mn aluminum alloy escalated in correlation with the degree of deformation. While the extent of improvement remains relatively inconspicuous, the subsequent aging treatment has the potential to enhance the ultimate tensile strength.

Drawing from the aforementioned research background, it is apparent that aging treatment significantly amplifies the mechanical properties of cold-rolled specimens. Heightened deformation results in greater strength following the aging process when exposed to the invariable aging temperature. However, with scarce literature addressing the microstructure and mechanical properties of medium–heavy alloy after cold rolling and aging treatment, existing studies primarily concentrated on conventional low-density nonferrous metals. Consequently, this paper, expanding on prior research [15], carries out aging treatment on cold-rolled medium–heavy alloys (90% deformation). With the aim of offering technical support for the production of medium–heavy alloys with outstanding comprehensive mechanical properties, the study systematically examines the development of microstructure and mechanical properties of medium–heavy alloys after various aging times.

2. The Experimental Materials and Research Methods

The experimental materials with element composition of 38.53% W, 5.09% Co, 0.97% Ta, and remaining Ni were obtained by Vacuum induction melting (VIM) and Vacuum arc remelting (VAR). The specific preparation procedure is described in Reference [15]. The novel heat-treated Ni-W-Co-Ta high-density alloy was cut into plate specimens of 100 mm × 40 mm × 10 mm along the forging direction for cold rolling. The reduction amount was about 2% in every pass, and the total cumulative deformation was 90%.

The cold-rolled sheets were aged in a tubular high-temperature resistance furnace at 700 °C at various times (2 h, 4 h, 8 h, 16 h, 24 h, 32 h) and aircooled to room temperature. The phase composition analysis of the Ni-W-Co-Ta medium–heavy alloy after aging was conducted by X-ray diffraction (XRD) D8ADVANCE possessing tube current of 40 mA and voltage of 40 kV, with an angular span from 30° to 100°and incremental step size of 0.02. Following this, the sample underwent grinding and polishing and was then subjected to corrosion using a mixture of 20 mL nitric acid and 60 mL hydrochloric acid for 510 s. After being ground and polished, the microstructure of the sample, which was corroded in a mixture of 20 mL nitric acid and 60 mL hydrochloric acid for 510 s, was observed using an OLYMPUSPMG3 optical microscope (OM). A 10 mm × 10 mm × 1 mm sheet was intercepted parallel to the deformation direction, and a Φ3 mm wafer was punched out after mechanical grinding to 70 μm. The microstructure of the wafer that was thinned subsequently using the Gatan691 ion thinning instrument was characterized with the JEM2010 transmission electron microscope. Lastly, the average microhardness, with five points measured for each sample of the alloy before and after aging treatment, was quantified using the HVS-1000A digital.

The mechanical properties of the specimens were evaluated both before and after aging treatment utilizing the Instron 5587 tensile testing machine, with sample dimensions as depicted in Figure 1. Furthermore, the fracture morphology was meticulously examined using the JSM-7800F field emission-scanning electron microscope.

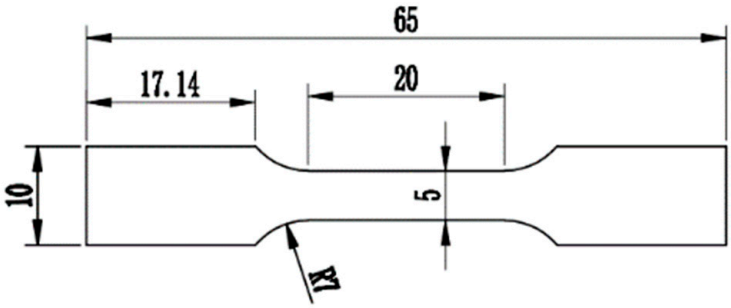

Figure 1. Dimensions of sample in millimeters (mm) for tensile specimens (thickness is 1 mm).

3. Results and Analysis

3.1. XRD Analysis

The X-ray diffraction (XRD) patterns and dislocation density of the Ni-W-Co-Ta medium–heavy alloy following aging treatments at 700 °C for varying aging times are showcased in Figure 2. Clearly, the emergence of new diffraction peaks corresponding to a novel phase, which is proven to be Ni_4W, with respective volume fractions of 13.7%, 16.3%, 18.6%, 23.1%, 26.4%, and 28.7% following aging times of 2 h, 4 h, 8 h, 16 h, 24 h, and 32 h, by comparing analysis with the PDF card (65–2673) is discernible from the sample (90% deformation), as shown in Figure 2a. Notably, a rightward shift of the XRD peaks of the cold-rolled Ni-W-Co-Ta medium–heavy alloy appears after prolonged high-temperature aging treatment because of the occurrence of recovery and recrystallization that results in lessened dislocation density, reduced residual internal stress, and a certain degree of grain growth. That the full width at half maximum (FWHM) of XRD diffraction peaks is inversely related to the grain size from the Scherrer formula [16] reveals the increased grain size with enhancive aging time from the trend that the FWHM of the diffraction peak gradually decreases under various aging times (2, 4, 8, and 16 h) from Figure 2b. However, an unusual FWHM broadening increase after 24 and 32 h originated from the peak overlap ((211) from Ni_4W and the (111) of $Ni_{17}W_3$) happens. The broadening of the (211) of β phase diffraction peak in the TB17 titanium alloy after aging at 350 °C is also due to the overlap of characteristic peaks of the newly formed phase and β phase is similar to this study [14].

It can be observed that the dislocation density of the cold-rolled samples continuously declines with prolonged aging time in Figure 2c. The number of corresponding dislocation densities is calculated from the average grain size and microstrain, as shown in Equation (1) [17]. In the unaged sample, the dislocation density of the experimental steel is 1.46×10^{15} m^{-2}. After aging treatments of 2 h, 4 h, 8 h, 16 h, 24 h, and 32 h, the dislocation density of the cold-rolled high-density alloy gradually decreases to 1.279×10^{15} m^{-2}, 1.163×10^{15} m^{-2}, 1.011×10^{15} m^{-2}, 9.7×10^{14} m^{-2}, 8.71×10^{14} m^{-2}, and 8.28×10^{14} m^{-2}, respectively.

$$\rho = \frac{2\sqrt{3}\left(\varepsilon^2\right)^{\frac{1}{2}}}{Db} \quad (1)$$

where ρ is the dislocation density, ε denotes the microscopic strain, D represents the average grain size, b is the Berger vector.

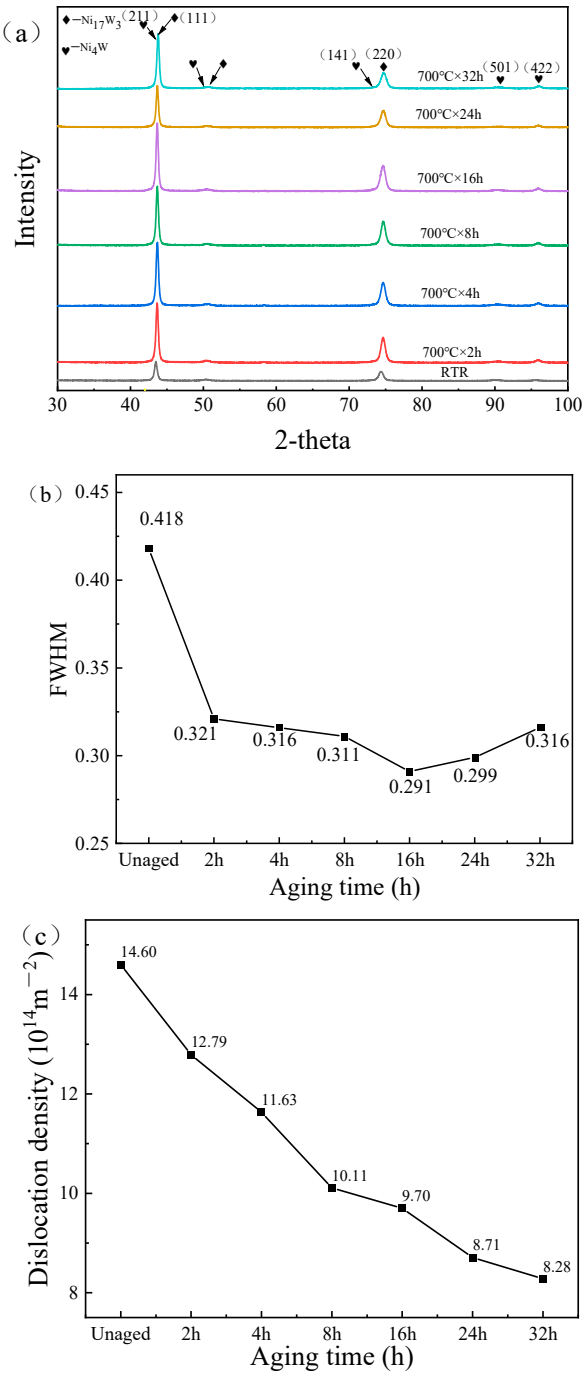

Figure 2. (**a**) XRD patterns; (**b**) FWHM and (**c**) dislocation density of cold-rolled samples after different aging time treatments at 700 °C.

3.2. OM Analysis

Figure 3 depicts the microstructure of the cold-rolled Ni-W-Co-Ta medium–heavy alloy subsequent to aging treatments at 700 °C for varying times. Following severe 90% cold-rolling deformation, the grains of the Ni-W-Co-Ta medium–heavy alloy undergo elongation along the rolling direction, rendering them arduous to differentiate. Simultaneously, the proliferation of slip bands occurs, leading to the partitioning of grains into diminutive units due to the interactions between adjacent slip bands, alongside the presence of a small number of undissolved tungsten particles in various configurations (elongated strips along the rolling direction, fractured into spherical and spindle shapes) at the grain boundaries [10]. After a 2 h aging treatment, the interaction between the slip bands disappeared, but the

matrix still showed elongated fiber texture morphology along the rolling direction, and the undissolved tungsten particles showed spherical distribution on the matrix, as shown in Figure 3a. Extending the aging time to 4 h yields the typical microstructure that remains largely unchanged compared to the 2 h aging time, as depicted in Figure 3b. Additionally, the quantity of slip bands diminishes visibly, making them challenging to discern, while the fibrous structure undergoes a degree of coarsening after aging treatment, and the recovery areas can be clearly observed, lasting 8 h in Figure 3c. The decreased number of slip bands continues, and the interactions between them gradually dissipate, resulting in the matrix adopting an elongated fibrous morphology along the rolling direction with a further increase in aging time to 16 h, as evidenced in Figure 3d. The matrix retains its fibrous organizational characteristics following a 24 h aging treatment, at which point the slip bands nearly vanished and the proportion of recovery areas increased (Figure 3e). With the aging time increasing to 32 h, the morphology of the fibrous structure gradually becomes less distinct, and the proportion of the recovery areas further increased, intensifying the phenomenon of grain recovery, as depicted in Figure 3f.

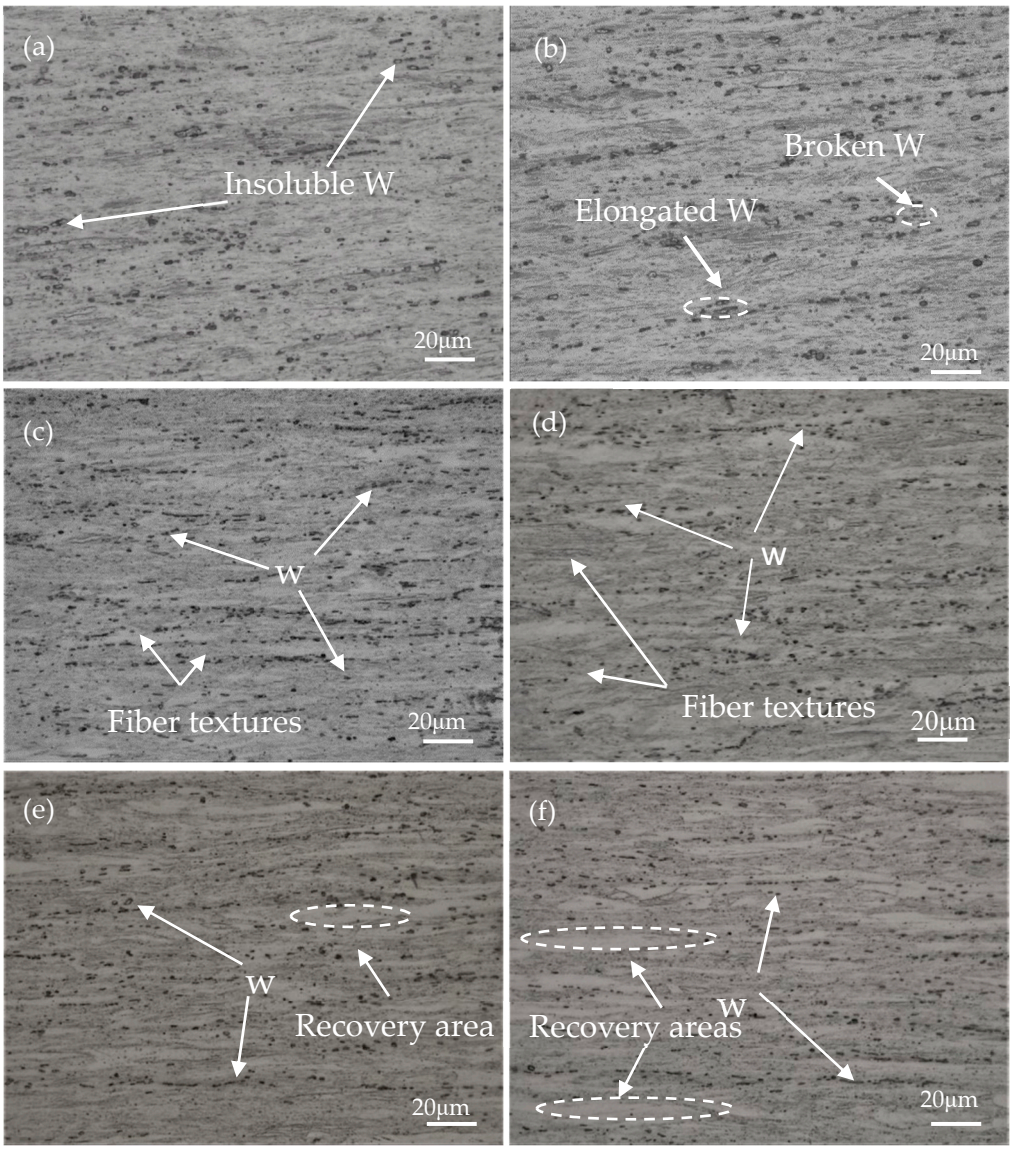

Figure 3. Microstructural morphology of cold-rolled samples after different aging time treatments at 700 °C (**a**) 2 h; (**b**) 4 h; (**c**) 8 h; (**d**) 16 h; (**e**) 24 h; (**f**) 32 h.

3.3. TEM Analysis

In Figure 4a,b, the bright-field image and the corresponding darkfield image of the cold-rolled Ni-W-Co-Ta medium–heavy alloy are presented after the 2 h aging treatment at 700 °C. Notably, the upper right corner of Figure 4a reveals the selected area electron diffraction (SAED), demonstrating the diffraction spot of the $Ni_{17}W_3$ phase in the matrix along the [001] band axis, accompanied by additional weak spots. The faint spots (marked with red circles) represent the W particles, while the brighter spots (marked with yellow circles) represent the Ni_4W, which were confirmed by calibrating the diffraction spots. As the aging treatment progresses, the diffraction spots of W atoms gradually diminish while those of the Ni_4W phase intensify. This phenomenon arises from the strong short-range order of W atoms in the Ni matrix within the cold-rolled medium–heavy alloy. Subsequent to aging treatment, this order gradually dissipates, leading to the precipitation of the Ni_4W phase [9].

An image of the distribution of the precipitated phase with an average size measuring 6.74 nm is shown in Figure 4b. A situation unfolds after embarking on a 4 h aging treatment: the dislocation density wanes, the quantity of the precipitated phase increases, and the average grain size expands to 7.6 nm, as shown in Figure 4c,d. Upon extending the aging time to 8 h, the dislocation density further decreases, the short-range ordering of W atoms dissipates, and the diffraction spots of the Ni_4W phase (size: approximately 8.84 nm) become more pronounced, as depicted in Figure 4e,f. Subsequent to the 16 h aging time, the recovery areas incur a reduction in lattice distortion, internal stress, and dislocation density. Ni-W-Co-Ta medium–heavy alloys are in a thermodynamically unstable high free-energy state due to the increase in the density of structural defects such as vacancies and dislocations and the elevation of the distortion energy, which has the tendency to recover to the low free-energy state before the deformation, but the recovery is slow at room temperature because of the low temperature and small atomic mobility. However, when the alloy is at the aging temperature, the atomic diffusion ability is enhanced, and with the extension of the aging time, more atoms undergo diffusion and gradually migrate to the equilibrium position, the number of vacancies decreases, the degree of lattice distortion decreases, and the internal stress is released. At the same time, the growing dislocations are slipped and rearranged, the heterologous dislocations on the same slip surface can be attracted to each other and offset, and the two dislocation lines of the dislocation dipole offset, with dislocations predominantly existing in the microstructure in low-energy dislocation entanglement and dislocation walls [18], as illustrated in Figure 4g. In Figure 4h, a rise in the quantity of precipitation is observed, while the grain size undergoes minimal change, measuring approximately 9.4 nm. The recovery becomes more apparent, with the dislocation density continuing to decrease, the quantity of the precipitation displaying dispersed distribution and showing a typical increased trend of the size of the precipitated phase expanding to 10.64 nm (24 h) and 11.52 nm (32 h) as the aging time extends to 24 and 32 h. Evidently, the dislocation density of cold-rolled samples gradually decreases, and the quantity and size of the precipitation expand with the growing aging time at the same temperature, as depicted in Figure 4i–l.

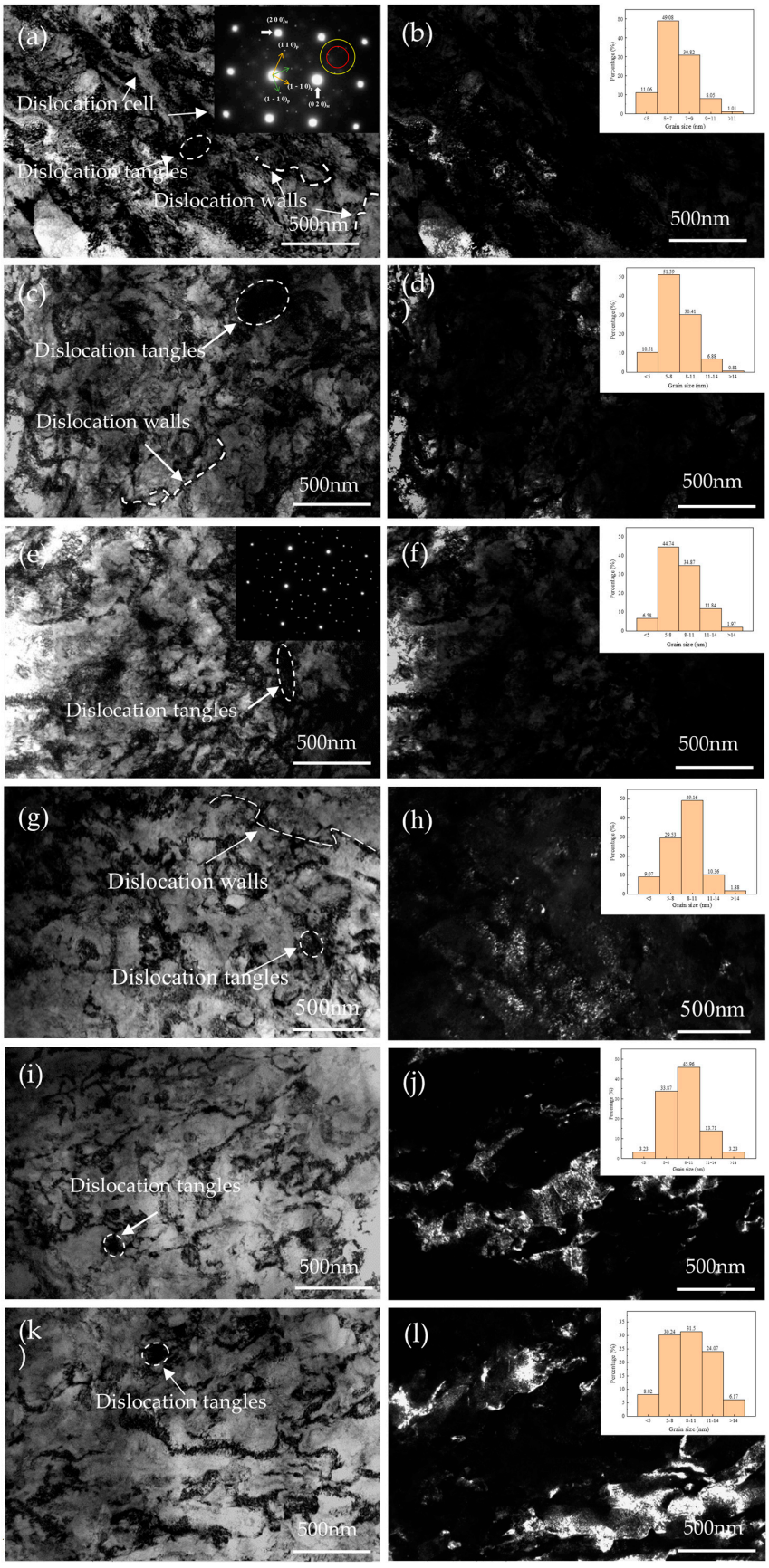

Figure 4. TEM images of cold-rolled samples after different aging time treatments at 700 °C (**a**,**b**) 2 h; (**c**,**d**) 4 h; (**e**,**f**) 8 h; (**g**,**h**) 16 h; (**i**,**j**) 24 h; (**k**,**l**) 32 h.

3.4. Microhardness

The microhardness of the 90% deformation rolled sample both before and after aging treatment at 700 °C for varying times is presented in Figure 5. Following the aging treatment, the microhardness of the cold-rolled specimen experiences an initial surge followed by a gradual decline with the extension of aging time. The microhardness of the sample undergoes a rapid ascent from 584 HV before aging to 687 HV after the aging treatment under 2 h. This increase in hardness is attributed to the precipitation of the Ni_4W, a brittle and hard phase, during the aging process. In addition, the microhardness of the specimens gradually ascends to 719 HV (4 h), 735 HV (8 h), and 766 HV (16 h) with the progression of aging time, which is primarily driven by the incremental precipitation of the Ni_4W phase, leading to an amplified precipitation strengthening effect. At the same time, the combined influence of reduced dislocation density further released residual internal stress, and the Ni_4W precipitation with augmented size leads to the regression of microhardness (725 HV and 706 HV) as the aging time extends to 24 h and 32 h.

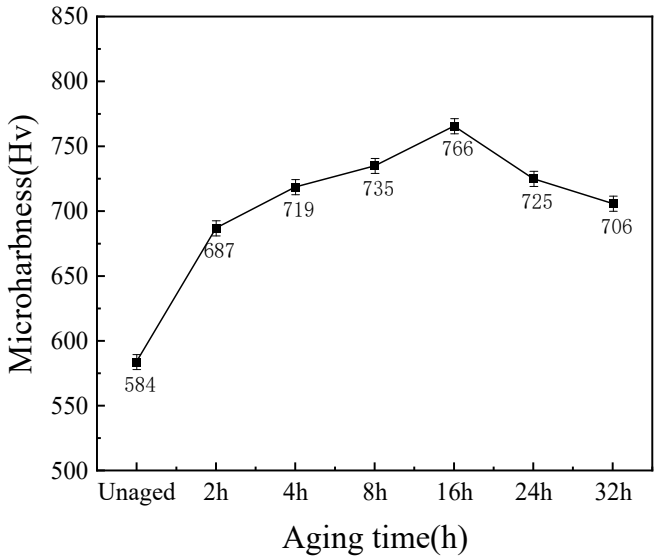

Figure 5. Microhardness of cold-rolled samples after different aging time treatments at 700 °C.

3.5. Strength and Elongation

The strength and elongation of the cold-rolled alloy before and after aging treatment are presented in Figure 6. Following the aging treatment, the strength of the cold-rolled samples embarks on the same trend as microhardness, experiencing an initial surge followed by a gradual decline as the aging time extends. The maximum is reached under the aging treatment (temperature: 700 °C; aging time: 16 h), where the tensile strength soars to 2286 MPa (UTS) and the yield strength ascends to 1989 MPa (YS). However, a contrary tendency emerges for elongation. This phenomenon finds its roots in the simultaneous precipitation and growth of the second phase, recovery of cold-rolled microstructure, and recrystallization processes in aging precipitated alloy after cold deformation [19–21] after aging treatment. In the aging process, the alloy has two reactions: recovery and precipitation of Ni_4W (hard and brittle phase). After 2 h of aging treatment, the strength and hardness increase significantly while the toughness decreases, indicating that the second precipitation phase has begun to form inside the alloy after a short aging treatment. The dislocations bypass the precipitation phase and need a certain amount of shear stress, and the dislocation resistance of the material increases, contributing to improved strength and hardness. At the same time, recovery occurs in some regions. The atoms gradually migrate to the equilibrium position because of enhanced diffusion ability, generating a reduced number of vacancies, a decreased degree of lattice distortion, released internal stress, and a lessened dislocation density. However, the effect of recovery is weak, and the second phase

of strengthening dominates. With the extension of aging time, the matrix continues to precipitate more second phase, and the effect of recovery is still replaced by the dispersion strengthening of the second phase. The strength and hardness continue to rise, and the toughness continues to decline; when aging time reaches 16 h, the content of precipitated phases gradually increases, but the enhancement of strength and hardness also becomes weaker. According to the second phase strengthening theory, after the nucleation of the precipitated phase grows up to the critical size, it is characterized as an undeformable particle, and the relationship between its strength increment and the volume fraction of the second phase and the particle size is as follows [22]. (Equation (2)):

$$YS_{PO} \propto f^{1/2} d^{-1} \cdot \ln d \quad (2)$$

where YS_{PO} denotes the strength increment; f represents the volume fraction of the second phase; d is the particle size. When the particle grows to the critical size, the volume fraction of the precipitated phase gradually weakens its strengthening effect, and finally, the strength and hardness of the alloy start to decrease under the combined effect of the coarsening of the precipitated phase and the recovery effect [23]. Moreover, Figure 6 unveils the continuous decline in elongation as the aging time prolongs in medium–heavy alloys, owing to the amplified precipitation of the hard phase (Ni_4W). This increase in lattice mismatch creates the condition for crack generation during the stretching process, ultimately leading to a decline in elongation.

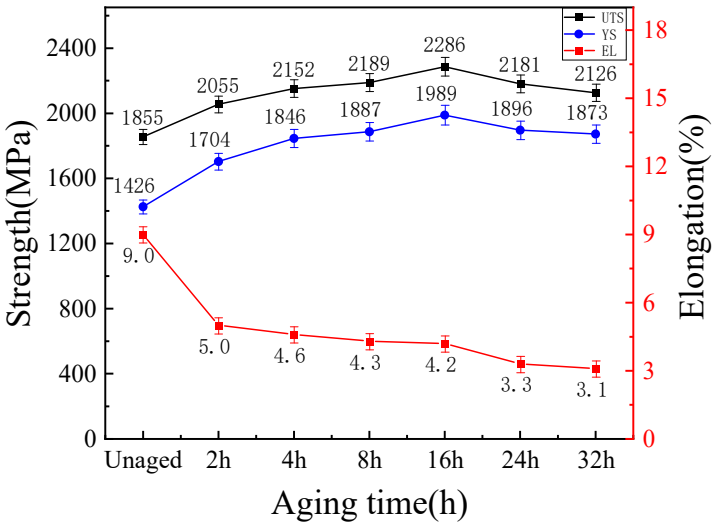

Figure 6. Strength and elongation of cold-rolled samples after different aging time treatments at 700 °C.

3.6. Fracture Morphology

Figure 7 exhibits the tensile fracture morphology of the cold-rolled specimen after varying aging time treatment at 700 °C. There is a reduction in dimple size, an increase in the number of micropores, and an expansion of the cleavage surface area following a 2 h aging treatment. And the dimples and micropores exhibit few alterations, while the cleavage surface area continues to expand upon extending the aging time to 4 h, as illustrated in Figure 7b. Following 8 h aging treatment, dimples become challenging to recognize due to their diminished size and shallower depth, with a further increase in the cleavage surface area (shown in Figure 7c). Furthermore, the section becomes irregular, the quantity of micropores escalates, and the cleavage surface area expands when the aging time reaches 16 h, as demonstrated in Figure 7d. In contrast to the morphology after 16 h of aging, the dimple size increases, but their depth diminishes, leading to a decrease in the cleavage surface area under a 24 h aging period, as depicted in Figure 7e. Upon extending the aging time to 32 h, the cleavage surface area continues to decrease, while the dimpled

morphology remains largely unaltered, as evidenced in Figure 7f. Ni-W-Co-Ta medium–heavy alloys have organizational inhomogeneity after cold rolling, which is mainly affected by grain orientation, and because this inhomogeneity makes the energy stored in different regions differ, the distribution of the second phase in the aging process is not uniform. Due to the presence of the second phase, this will hinder the dislocation movement, leading to the precipitation-hardening effect. Hence, some areas possess high strength but low ductility, causing cleavage fracture. In another part of the region, with relatively good ductility due to the recovery of the aging process, ductile fracture occurs. Therefore, the fracture morphology is characterized by ductile–brittle mixed fracture.

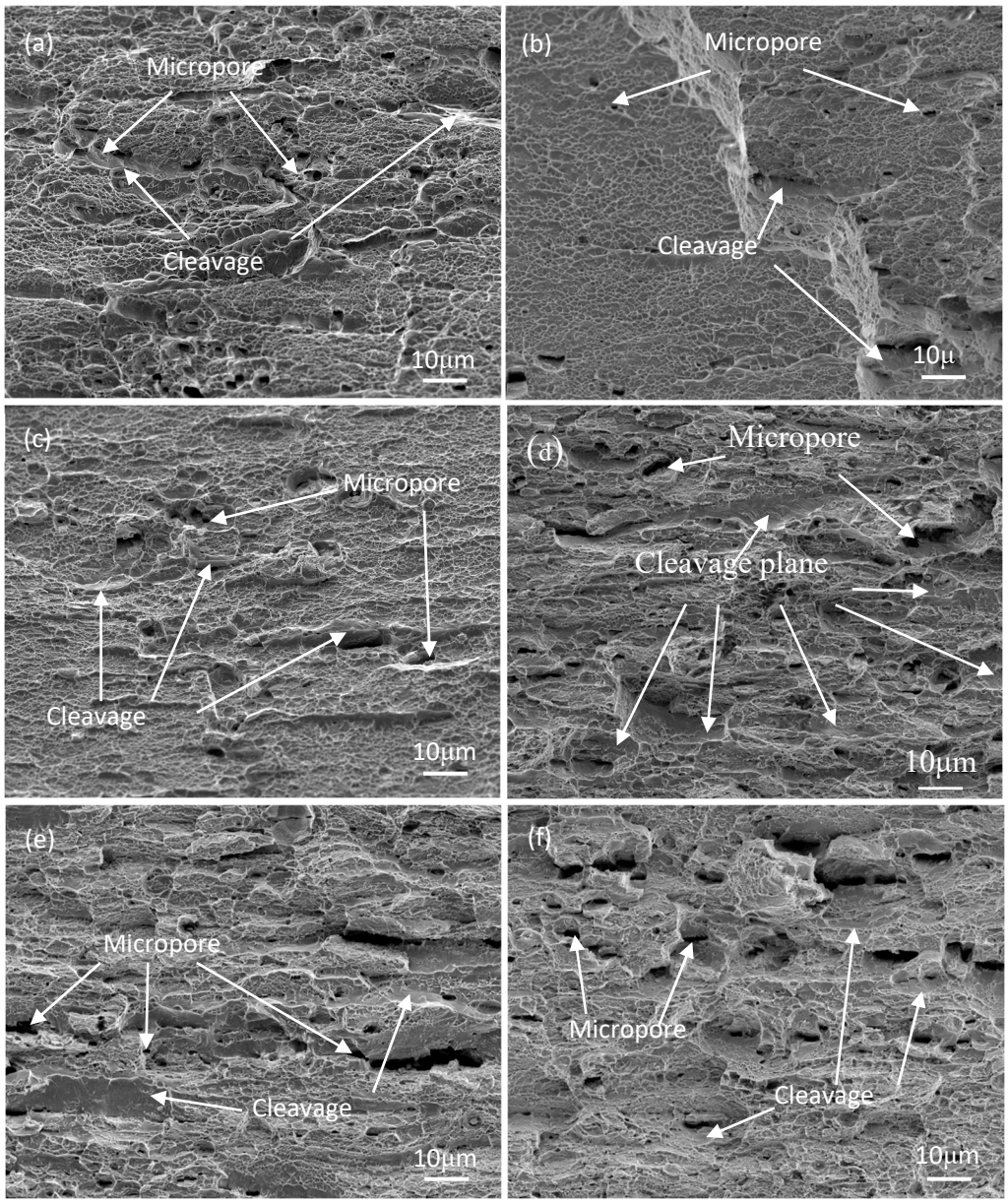

Figure 7. Fracture morphology of cold-rolled samples after different aging time treatments at 700 °C (**a**) 2 h; (**b**) 4 h; (**c**) 8 h; (**d**) 16 h; (**e**) 24 h; (**f**) 32 h.

4. Conclusions

This investigation delves comprehensively into the influence of aging time on the microstructure and mechanical properties of the cold-rolled Ni-W-Co-Ta medium–heavy alloy. The ensuing conclusions unfold as follows:

1. The aging process triggers the precipitation of the Ni_4W phase from the cold-rolled medium–heavy alloy. The Ni_4W phase reaches a size of about 11.52 nm, accompanied by a proportional increase in volume fraction to 28.7% as the aging time progresses from 2 h to 32 h.
2. Prolonged aging treatment of the cold-rolled Ni-W-Co-Ta medium–heavy alloy results in alleviated lattice distortion resulting from severe deformation, reduced internal stresses within grains, and decreased dislocation density, notably characterized by dislocation entanglement and dislocation walls within the microstructure.
3. The cold-rolled Ni-W-Co-Ta medium–heavy alloy attains maximum hardness, tensile strength, and yield strength at 766 HV, 2286 MPa (UTS), and 1989 MPa (YS), respectively, following the 16 h aging treatment at 700 °C.
4. After the aging treatment, the fracture morphology of the cold-rolled Ni-W-Co-Ta medium–heavy alloy exhibits a distinctive ductile–brittle mixed fracture characteristic.

Author Contributions: Writing-original draft preparation, Y.L.; writing-review and editing, Y.L. and Y.X.; visualization, H.-f.L. and Y.X.; supervision, S.H.; project administration, F.-z.R.; funding acquisition, Y.L., Y.X. and C.-x.W. All authors have read and agreed to the published version of the manuscript.

Funding: This work was supported by the National Key Research and Development Plan (2022YFB3705200), the Major science and technology projects of Henan Province (221100230200), National Natural Science Foundation of China (U1804146, 51905153, and 52111530068).

Data Availability Statement: The datasets generated during and/or analyzed during the current study are available from the corresponding author upon reasonable request.

Conflicts of Interest: The authors declare that they have no known competing financial interests or personal relationships that could have appeared to influence the work reported in this article.

References

1. Sharma, V.; Namburu, S.A.S.; Lalwani, P.; Sagar, C.K. Constitutive modelling and processing map analysis of tungsten heavy alloy (92.5W-5.25Ni-2.25Fe) at elevated temperatures. *Int. J. Refract. Met. Hard Mater.* **2018**, *76*, 168–179. [CrossRef]
2. Chuvildeeva, V.N.; Nokhrina, A.V.; Boldina, M.S.; Sakharova, N.V.; Baranovb, G.V. Influence of high-energy ball milling on the solid-phase sintering kinetics of ultrafine-grained heavy tungsten alloy. *Dokl. Phys.* **2017**, *62*, 420–424. [CrossRef]
3. Kiran, U.R.; Venkat, S.; Rishikesh, B.; Iyer, V.K.; Sankaranarayana, M.; Nandy, T.K. Effect of tungsten content on microstructure and mechanical properties of swaged tungsten heavy alloys. *Mater. Sci. Eng. A* **2013**, *528*, 389–396. [CrossRef]
4. Prabhu, G.; Kumar, N.A.; Sankaranarayana, N.A.; Nandy, T.K. Tensile and impact properties of microwave sintered tungsten heavy alloys. *Mater. Sci. Eng. A* **2014**, *607*, 63–70. [CrossRef]
5. Senthilnathan, N.; Annamalai, A.R.; Venkatachlam, G. Microstructure and mechanical properties of spark plasma sintered tungsten heavy alloys. *Mater. Sci. Eng. A* **2018**, *710*, 66–73. [CrossRef]
6. Haag, J.V.; Edwards, D.J.; Henager, C.H.; Setyawan, W.; Wang, J.; Murayama, M. Characterization of ductile phase toughening mechanisms in a hot-Rolled tungsten heavy alloy. *Acta Mater.* **2021**, *204*, 116523. [CrossRef]
7. Zhang, X.Q.; Li, S.K.; Liu, J.X.; Wang, Y.C.; Wang, X. Self-sharpening behavior during ballistic impact of the tungsten heavy alloy rod penetrators processed by hot-hydrostatic extrusion and hot torsion. *Mater. Sci. Eng. A* **2010**, *527*, 4881–4886.
8. Gong, X.; Fan, J.L.; Ding, F.; Song, M.; Huang, B.Y.; Tian, J.M. Microstructure and highly enhanced mechanical properties of fine-grained tungsten heavy alloy after one-pass rapid hot extrusion. *Mater. Sci. Eng. A* **2011**, *528*, 3646–3652. [CrossRef]
9. Li, Y.; Liu, G.Q.; Hu, X.B.; Wu, L.H.; Tan, C.W.; Dravid, V.P.; Liu, S.Z. A novel medium heavy alloy with superior quasi-static and dynamic properties. *Scripta Mater.* **2019**, *162*, 311–315. [CrossRef]
10. Xiong, Y.; Shu, K.-H.; Li, Y.; Chen, Z.-G.; Zha, X.-Q.; He, T.-T.; Han, S.; Wang, C.-X. Deformation temperature impacts on the microstructure evolution and mechanical properties of a novel medium-heavy alloy (MHA). *Mater. Sci. Eng. A* **2022**, *856*, 144005. [CrossRef]
11. Zhang, K.; Yang, J.; Li, J.; Chen, X.; Zhou, H.; Liu, P. Effect of deformation and aging treatment on the microstructure and properties of Cu-0.45Cr-0.14Ti (wt.%) alloy. *J. Alloys Compd.* **2021**, *851*, 156776. [CrossRef]
12. He, F.; Yang, S.; Cao, J. Effect of cold rolling and aging on the microstructure and mechanical properties of Ti-Nb-Zr Alloy. *J. Mater. Eng. Perform.* **2020**, *29*, 3411–3419. [CrossRef]
13. Sadeghi-Nezhad, D.; Anijdan, S.M.; Lee, H.; Shin, W.; Park, N.; Nayyeri, M.; Jafarian, H. The effect of cold rolling, double aging and overaging processes on the tensile property and precipitation of AA2024 alloy. *J. Mater. Res. Technol.* **2021**, *9*, 15475–15485. [CrossRef]

14. Luo, J.-M.; Zhu, H.-C.; Zhu, Z.-S.; Xu, J.-L.; Li, M.-B. Phase precipitation behavior of TB17 titanium alloy during isothermal aging process. *Rare Metal Mater. Eng.* **2021**, *50*, 3862–3870.
15. Shu, K.H.; Xiong, Y.; Li, Y.; Zhang, X.; Yin, L.-T.; Ren, F.-Z. Effect of cold rolling on microstructure and properties of a novel Ni-W-Co-Ta heavy alloy. *Rare Metal Mater. Eng.* **2023**, *52*, 3833–3839.
16. Li, Z.-B.; Zhang, H.; Chen, B.; Zhang, G.-H.; Chou, K.-C. Microstructure and mechanical properties of Al_2O_3 dispersed fine-grained medium heavy alloys with a superior combination of strength and ductility. *Mater. Sci. Eng. A* **2021**, *817*, 141376. [CrossRef]
17. Cheng, H.; Wang, H.Y.; Xie, Y.C.; Tang, Y.C.; Dai, Y.C. Controllable fabrication of a carbide-containing FeCoCrNiMn high-entropy alloy: Microstructure and mechanical properties. *Mater. Sci. Eng.* **2017**, *33*, 2032–2039. [CrossRef]
18. Grässel, O.; Frommeyer, G. Effect of martensitic phase transformation and deformation twinning on mechanical properties of Fe-Mn-Si-AI steels. *J. Mater. Sci. Technol.* **1998**, *14*, 1213–1217. [CrossRef]
19. Deng, Y.-J.; Huang, G.-J.; Cao, L.-F.; Wu, X.-D.; Huang, L.; Xia, M.-Y.; Liu, Q. Improvement of strength and ductility of Al-Cu-Li alloy through cryogenic rolling followed by aging. *T. Nonferr. Metal. Soc.* **2017**, *27*, 1920–1927. [CrossRef]
20. Li, C.; Xiong, H.Q.; Bhatta, L.; Wang, L.; Zhang, Z.Y.; Wang, H.; Kong, C.; Yu, H.L. Microstructure evolution and mechanical properties of Al-3.6Cu-1Li alloy via cryorolling and aging. *T. Nonferr. Metal. Soc.* **2020**, *30*, 2904–2914. [CrossRef]
21. Jayaganthan, R. Effects of warm rolling and ageing after cryogenic rolling on mechanical properties and microstructure of Al 6061 alloy. *Mater. Des.* **2012**, *39*, 226–233.
22. Brigham, R.J.; Tozer, E.W. Effect of alloying on pitting resistance of 18% Cr austenitic stainless steels. *Corrosion* **1974**, *30*, 161–166. [CrossRef]
23. He, X.; Pan, Q.; Li, H.; Huang, Z.; Liu, S.; Li, K.; Li, X. Effect of artificial aging, delayed aging, and pre-aging on microstructure and properties of 6082 aluminum alloy. *Metals* **2019**, *9*, 173. [CrossRef]